Journal of Biomedical Optics

BiomedicalOptics.SPIEDigitalLibrary.org

Optimization of the method for assessment of brain perfusion in humans using contrast-enhanced reflectometry: multidistance time-resolved measurements

Daniel Milej
Dariusz Janusek
Anna Gerega
Stanislaw Wojtkiewicz
Piotr Sawosz
Joanna Treszczanowicz
Wojciech Weigl
Adam Liebert

SPIE.

Optimization of the method for assessment of brain perfusion in humans using contrast-enhanced reflectometry: multidistance time-resolved measurements

Daniel Milej,[a,*] Dariusz Janusek,[a] Anna Gerega,[a] Stanislaw Wojtkiewicz,[a] Piotr Sawosz,[a] Joanna Treszczanowicz,[b] Wojciech Weigl,[b,c] and Adam Liebert[a]
[a]Polish Academy of Sciences, Nalecz Institute of Biocybernetics and Biomedical Engineering, 4Ks. Trojdena Street 02-109 Warsaw, Poland
[b]Warsaw Praski Hospital, Department of Intensive Care and Anesthesiology, 67 Al. Solidarnosci Street, 03–401 Warsaw, Poland
[c]Uppsala University, Department of Surgical Sciences/Anesthesiology and Intensive Care, 751 85 Uppsala, Sweden

Abstract. The aim of the study was to determine optimal measurement conditions for assessment of brain perfusion with the use of optical contrast agent and time-resolved diffuse reflectometry in the near-infrared wavelength range. The source-detector separation at which the distribution of time of flights (DTOF) of photons provided useful information on the inflow of the contrast agent to the intracerebral brain tissue compartments was determined. Series of Monte Carlo simulations was performed in which the inflow and washout of the dye in extra- and intracerebral tissue compartments was modeled and the DTOFs were obtained at different source-detector separations. Furthermore, tests on diffuse phantoms were carried out using a time-resolved setup allowing the measurement of DTOFs at 16 source-detector separations. Finally, the setup was applied in experiments carried out on the heads of adult volunteers during intravenous injection of indocyanine green. Analysis of statistical moments of the measured DTOFs showed that the source-detector separation of 6 cm is recommended for monitoring of inflow of optical contrast to the intracerebral brain tissue compartments with the use of continuous wave reflectometry, whereas the separation of 4 cm is enough when the higher-order moments of DTOFs are available. [DOI: 10.1117/1.JBO.20.10.106013]

Keywords: time-resolved near-infrared measurements; diffuse reflectance; indocyanine green; brain imaging.

Paper 150531R received Aug. 7, 2015; accepted for publication Oct. 6, 2015; published online Oct. 28, 2015.

1 Introduction

Near-infrared spectroscopy (NIRS) is extensively tested as an optical method for assessment of the brain oxygenation in adults. Continuous wave,[1,2] frequency-domain,[3,4] and time-domain[5] measurement techniques were successfully applied in *in vivo* studies showing promising results. Functional NIRS (Ref. 6) allows for monitoring of oxygenation changes in the brain's cortex during a variety of stimulations in analogy to functional magnetic resonance imaging technique. Furthermore, recent studies showed that connectivity on the cortex can be studied by the application of dense grids of sources and detectors positioned on the surface of the head.[7–11] This advanced technique needs analysis of signals measured at multiple source-detector separations in order to minimize the influence of changes in oxygenation of the extracerebral tissue layers on the measured signals of changes in oxy- and deoxyhemoglobin.[12–16] A different optical technique that can be potentially used for intraoperative mapping of the human cortex during neurosurgery is the imaging of intrinsic optical signals.[17,18] This technique is based on measuring the intrinsic activity-related changes in tissue reflectance, caused by the functional physiological changes in blood volume, hemoglobin, or oximetry changes.

Another path of development of optical techniques for assessment of the cerebral perfusion represent studies in which the diffuse reflectance NIRS measurements were carried out during inflow and washout of indocyanine green (ICG).[19–21] Intravenous injection and monitoring of this optical contrast agent, which reveals strong absorption for near-infrared radiation, allows for assessment of brain perfusion, which is typically based on estimation of the time between injection and maximum of the dye concentration in the tissue under investigation.[22–27] Recently, it was reported that time-resolved spectroscopy may be of benefit for such brain perfusion studies.[28–30] It was shown that higher-order moments of the distributions of time of flight of photons (DTOFs) measured on the surface of the head (mean time of flight and variance of the DTOF) are more sensitive to the changes in absorption of the brain tissue related to the inflow of the ICG than total number of photons (zeroth-order moment of the DTOF), which reveals sensitivity to changes in absorption of the extracerebral tissue layers.[31,32] However, higher-order statistical moments of the DTOFs are sensitive to noise. This effect is especially pronounced in measurements carried out at large source-detector separations in which the number of detected photons is limited.[33,34]

The aim of the study was to evaluate the dependence of the signals related to the inflow of the ICG on the source-detector separation. This analysis will be presented in the context of optimization of the source-detector separation used in the estimation of the brain perfusion parameters. Optimized selection of the

*Address all correspondence to: Daniel Milej, E-mail: dmilej@ibib.waw.pl

1083-3668/2015/$25.00 © 2015 SPIE

statistical moments used in brain perfusion studies will also be discussed. Results of Monte Carlo (MC) simulations, phantom experiments, and *in vivo* tests carried out at multiple source-detector separations with the use of a time-resolved technique will be presented.

2 Methods

2.1 *Monte Carlo Simulations*

The MC code used for the study was described in detail earlier.[35–37] The algorithm allows for efficient simulations of DTOFs at different source-detector separations for different combinations of absorption properties of the layered medium. The statistical moments of the DTOFs related to the absorption coefficient change resulting from simulated inflow and washout of the ICG to two layers of the model (lower and upper) mimicking intra and extracerebral tissue compartments were analyzed. The temporal changes in absorption of the dye, μ_a, were simulated independently for both layers of the medium according to the functions proposed by Leung et al.[36,38] Initial optical properties of the medium were as follows: absorption coefficient of the medium $\mu_a = 0.015$ mm^{-1}, reduced scattering coefficient of the medium $\mu_s' = 1$ mm^{-1}, and refractive index $n = 1.4$. Initially, the superficial layer was assumed to be 1 cm thick and the deeper layer was 1 m thick (which simulates semi-infinite medium). Amplitudes of the changes of the absorption coefficient $\Delta\mu_a$ in the upper and lower layers were chosen in the range from 0.002 to 0.004 mm^{-1}. The DTOFs were obtained at 67 source-detector separations (from 0.1 to 6.7 cm). Because at the largest source-detector separations only a small number of photons are re-emitted, the simulations were carried out for a large total number of photon packages $N = 2 \times 10^9$.

2.2 *Instrumentation*

Time-resolved laboratory system based on eight photomultiplier tubes (PMT, R7400U−02, Hamamatsu Photonics, Japan) and eight time-correlated single photon counting (TCSPC) cards (SPC-134, Becker and Hickl, Berlin, Germany)[39–41] was used in combination with femtosecond MaiTai laser (Spectra Physics),[33,42] allowing the measurement of 16 DTOFs simultaneously. Laser pulses were generated at a wavelength of 760 nm with a frequency of 80 MHz. The wavelength used in the experiments was selected close to the maximum of the absorption spectrum of ICG and with consideration of the properties of filters used in order to block the fluorescence light.[21,36] The laser light was coupled into two fibers (1.5 and 3 m long, $\phi = 1$ mm, NA = 0.39) used to deliver the light to the phantom or the head of the healthy volunteer. Two beam expanders (F810SMA-780 and F220SMA-B, Thorlabs, Sweden) were applied on the tips of the source fibers in order to distribute the laser light on large areas of the tissue (15 and 8 mm diameter). This solution allowed us to keep the laser power density on the surface of the head below the safety limits (2 mW/mm^2). The laser light powers at the tips of the source fibers were 200 and 20 mW, respectively. Eight fiber bundles of diameter 7 mm with active area of diameter 4 mm (NA = 0.54, Loptek, Germany) were used to deliver the light re-emitted for the phantom or tissue to the photodetectors. The short-pass filters (NT47−586, Edmund Optics) with cut-off wavelength of $\lambda = 800$ nm were mounted in front of the PMTs in order to block the fluorescence light.

The combination of the two source positions and eight detection spots allowed for monitoring of optical signals for 16 source-detector separations in the range $r_{SD} = 10$ to 67.5 mm. The laser beam (output from MaiTai laser) was split into two light paths, which were coupled into two optical fibers. In this way, the laser pulses transmitted into the tissue or phantom using these two fibers were delayed by ≈3 ns.

2.3 *Phantom Experiments*

The phantom consisted of a fish tank (41 cm × 26 cm × 30 cm) filled with a 1:3 mixture of milk (fat content 3.2%) and water with small amount of ink (Black Indian Ink, Winsor & Newton). The solution of milk, water, and ink was used to obtain optical properties corresponding to properties of human tissue ($\mu_a \approx 0.035$ cm^{-1} and $\mu_s' \approx 12.5$ cm^{-1}). The optical properties of the medium were obtained by time-resolved measurements and by analysis of the statistical moments of the measured DTOFs.[43]

The measurements were carried out on the homogeneous phantom in which two transparent PVC tubes (inner diameter= 3 mm and outer diameter= 3.8 mm) were located at different depths (0 and 2 cm) with respect to the surface of the phantom. The measurements were carried out at 16 source-detector separations (see Fig. 1) by positioning the optodes holder equipped with two source fibers and eight detecting fiber bundles on the surface of the phantom.

In order to mimic dynamic inflow of the dye through the tubes located deeper and more superficial, a laboratory setup equipped with a peristaltic pump[44] was applied in order to pump through the tubes the same solution of milk, water, and ink that filled out the phantom. Furthermore, two independent boluses of ICG were injected into the two tubes located at different depths with a defined delay between them. First, the bolus was injected into the tube located deeper, which mimics realistic sequence of inflow of the bolus to the intra and extracerebral tissue compartments.

2.4 *In Vivo Measurements*

The *in vivo* measurements were carried out on three healthy volunteers (mean age 36, the coauthors of the paper). The

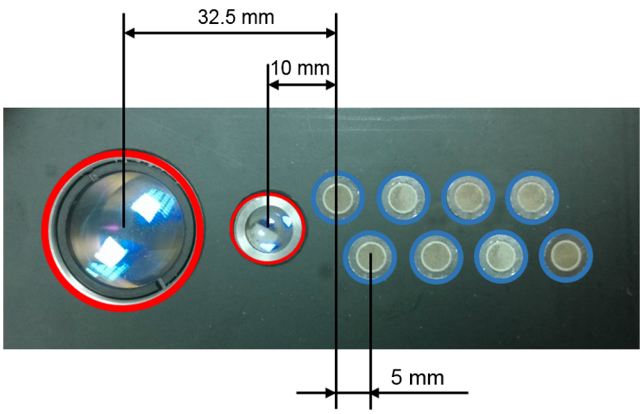

Fig. 1 The optode holder used in the phantom and *in vivo* studies. Red rings mark the positions of the beam expanders (source positions) and blue rings reflect locations of the tips of the detection fiber bundles.

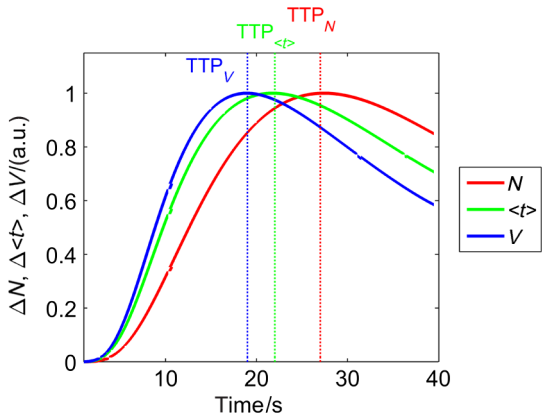

Fig. 2 Presentation of the data processing principle [time-to-peak (TTP) parameter calculation from the time-courses of the statistical moments of distribution of time of flights of photons (DTOFs)] on the data obtained by Monte Carlo (MC) simulations.

measurements protocol was approved by the Ethics Committee of the Medical University of Warsaw. In each case, a written informed consent was obtained from the subject. The subjects were examined in supine position. The optodes were fixed on the surface of the head with the use of rubber foam and Velcro stripes. The optodes were positioned on the right frontal area of the head below the line of hairs. A dose of 10 mg of ICG (Pulsion, Germany) dissolved in 5 mL of aqua pro injectione was administrated into the left forearm vein.

2.5 *Data Analysis*

In the preprocessing phase in the measured DTOFs, the background signal was subtracted and correction of nonlinearity of the TCSPC electronics was applied. The statistical moments of the simulated and measured DTOFs (number of photons N, mean time of flight $\langle t \rangle$, and variance V) were derived from the parts of the distributions limited by 3% of their maxima.[43] Time-courses of the statistical moments calculated for different source-detector separations were normalized and the time-to-peak (TTP) corresponding to the maximum of amplitude change caused by the ICG inflow was calculated. Typically the TTP values decrease with the order of the statistical moment ($TTP_N > TTP_{\langle t \rangle} > TTP_V$) as shown in Fig. 2.

In the next step, ΔTTP values for each statistical moment were calculated. In the case of MC simulations, ΔTTP was estimated as the difference between the calculated TTP values and reference value, which was TTP_0 obtained for simulated inflow function for the lower layer of the model.[38] In the phantom studies and *in vivo* measurements, the reference value TTP_0 was determined for each of the experiments as the minimal value of TTP_V. In the case of MC simulations, TTP_{MAX} was obtained by the analysis of the simulated inflow function for the upper layer of the model. In the phantom studies and *in vivo* measurements, the reference value TTP_{MAX} was determined for each experiment as the maximal value of TTP_N.

3 Results

3.1 *Monte Carlo Simulations*

Results of the analysis of ΔTTP obtained for different statistical moments of DTOFs calculated by MC simulations for different thickness of the upper layer (from 6 to 12 mm) are presented in Fig. 3. In these simulations, the reduced scattering coefficient was assumed to be $\mu_s' = 10\ \text{cm}^{-1}$. It should be noted that ΔTTP approaches zero when the simulated signal perfectly reveals

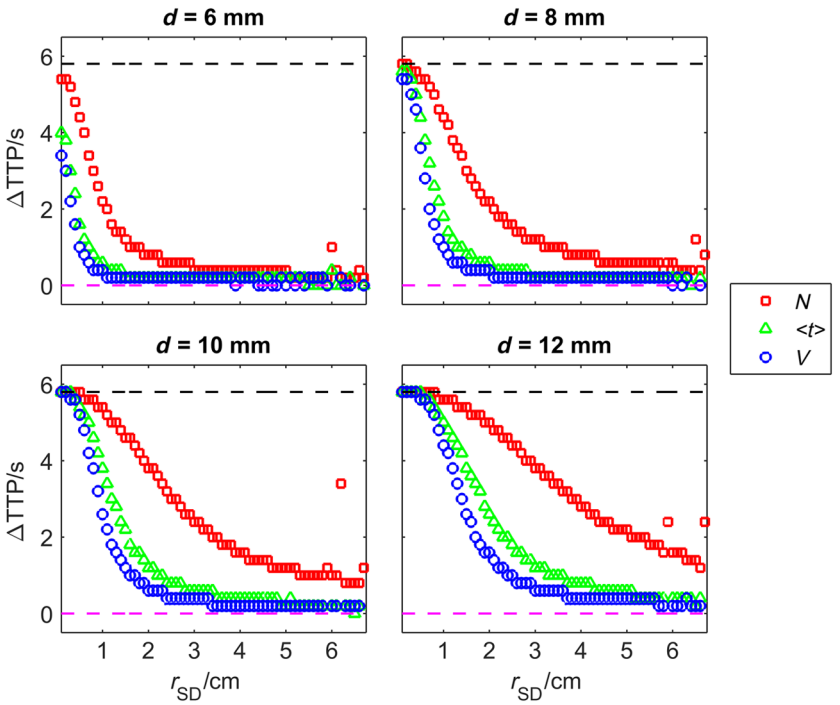

Fig. 3 Analysis of the results of the MC simulations. Changes in ΔTTP obtained at different source-detector separations and different upper layer thickness for three moments of DTOFs: total number of photons N, mean time of flight $\langle t \rangle$, and variance of the DTOF V. The reduced scattering coefficient was assumed to be $\mu_s' = 10\ \text{cm}^{-1}$.

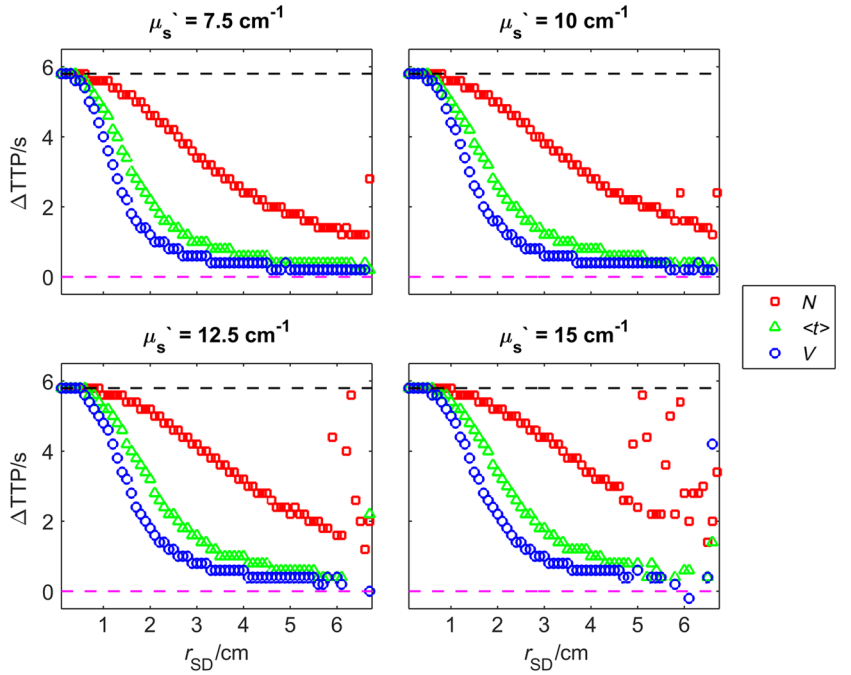

Fig. 4 Analysis of the results of the MC simulations. Changes in ΔTTP obtained at different source-detector separations and different reduced scattering coefficient of the medium for three moments of DTOFs: total number of photons N, mean time of flight $\langle t \rangle$, and variance of the DTOF V. The thickness of the upper layer was assumed to be 10 mm.

the inflow of the dye to the deeper layer of the model. It can be observed that for thin extracerebral tissue compartment, all statistical moments can provide information corresponding to the deeper tissue compartment even for source-detector separations <3 cm. However, increase in the thickness of the upper layer causes the ΔTTP obtained from the signals of the total number of photons N to be strongly overestimated. This effect, with lesser extent, can be observed for higher-order statistical moments. Only small discrepancy between the estimated and expected value of ΔTTP can be observed (<0.2 s) for source-detector separations $r_{SD} \geq 4$ cm when the variance V of the DTOF is analyzed.

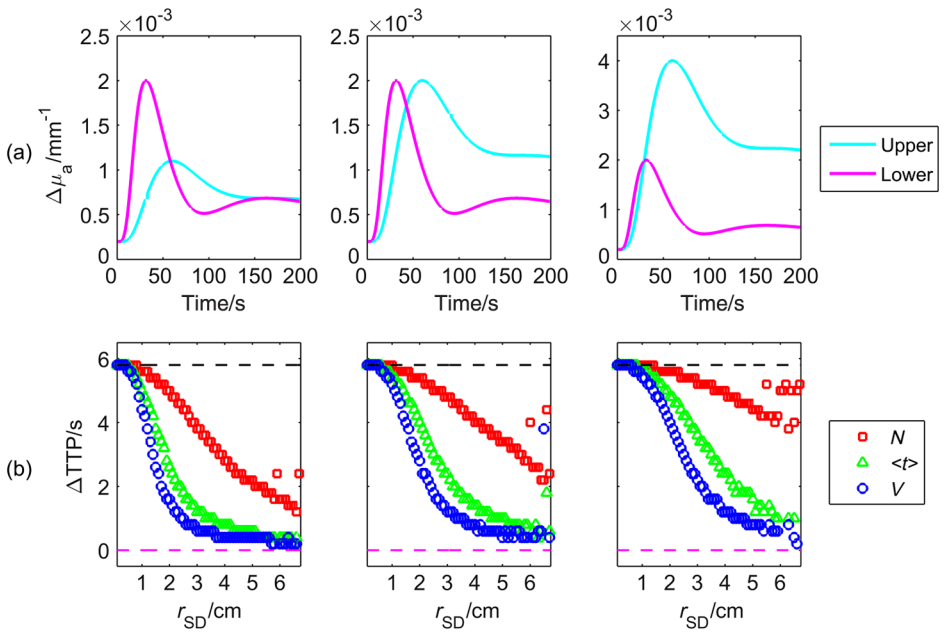

Fig. 5 Analysis of results of the MC simulations obtained for different amplitudes of change in absorption coefficient in the upper layer of the model. (a) Dynamic changes in absorption coefficient in upper and lower layer of the model and (b) corresponding changes in ΔTTP at different source-detector separations calculated for: total number of photons N, mean time of flight $\langle t \rangle$and variance $V$of the DTOFs. The thickness of the upper layer was assumed to be 10 mm and the reduced scattering coefficient was assumed to be $\mu_s' = 1$ mm^{-1}.

Results of the second series of MC simulations are presented in Fig. 4. Analysis of ΔTTP was carried out for media of different reduced scattering coefficient μ_s'. It can be observed that scattering properties of the medium strongly influence the sensitivity of the moments to the inflow of the dye to the deeper layer of the model. The increase in μ_s' leads to strong discrepancy between the estimated and expected value of ΔTTP when the total number of photons N is analyzed. This effect can also be observed for higher-order statistical moments, but this discrepancy remains relatively small (<1 s) for all values of μ_s' and large source-detector separations ($r_{SD} > 3$ cm) when the variance V of the DTOF is analyzed.

Results of the last series of MC simulations are presented in Fig. 5. Analysis of ΔTTP was carried out for different relations between amplitudes of changes in absorption of the dye μ_a for both layers of the model. It can be observed that increase in the amplitude of change in the absorption coefficient μ_a in the upper layer of the model results in increase in discrepancy of ΔTTP estimation. When the amplitude of change in the upper layer of the model is two times larger than that in the lower layer, the uncertainty of ΔTTP estimation is <1 s only for V signal obtained at source-detector separation >4 cm.

3.2 *Phantom Experiments*

The results of the phantom experiments are presented in Fig. 6. Obtained results show trends similar to those presented in the MC simulations. For larger delays between bolus appearance in the tubes located deeper and superficially, ΔTTP changes quickly with source-detector separation. Moreover, as expected, the uncertainty of ΔTTP estimation is lower when the delay in appearance of the boluses in the deeper and superficial tubes is larger.

3.3 *In Vivo Measurements*

The DTOFs were obtained for 16 source-detector separations (from 1 to 6.75 cm) during *in vivo* (see Fig. 7) tests carried out in healthy volunteers. As presented in Fig. 7, results of these experiments confirm the trends that were observed in MC simulations and phantom experiments.

As expected, the uncertainty of ΔTTP estimation is lowest when the V signal is analyzed. However, the decrease in the discrepancy observed in ΔTTP depends strongly on the subject measured.

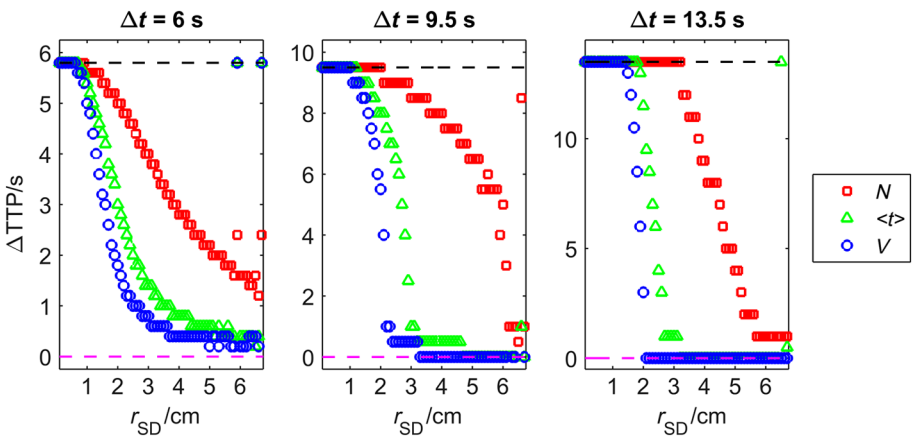

Fig. 6 Results obtained during phantom experiments. Changes in ΔTTP obtained at different source-detector separations for three delays Δt between the appearances of the boluses of indocyanine green (ICG) in the tubes located superficially and deeper in the medium. Results of the analysis of three moments of DTOFs: total number of photons N, mean time of flight $\langle t \rangle$, and variance V of the DTOF.

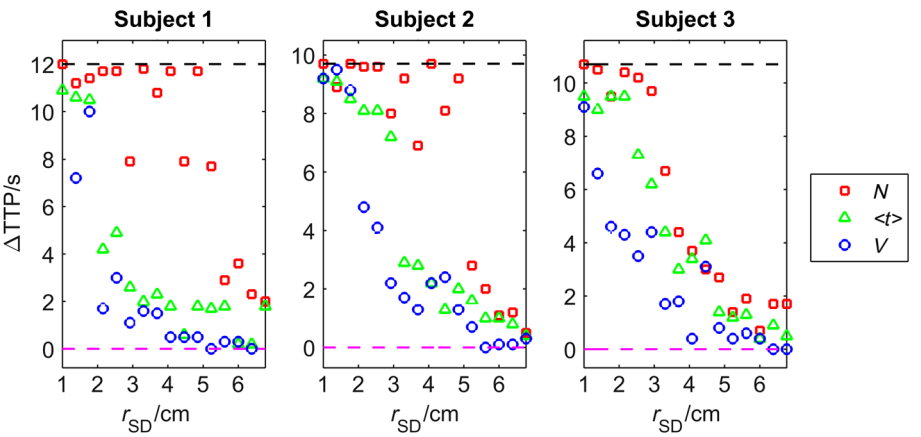

Fig. 7 Analysis of results of the *in vivo* experiments carried out on three healthy volunteers. Changes in ΔTTP obtained at different source-detector separations by analysis of three moments of DTOFs: total number of photons N, mean time of flight $\langle t \rangle$, and variance of the DTOF V.

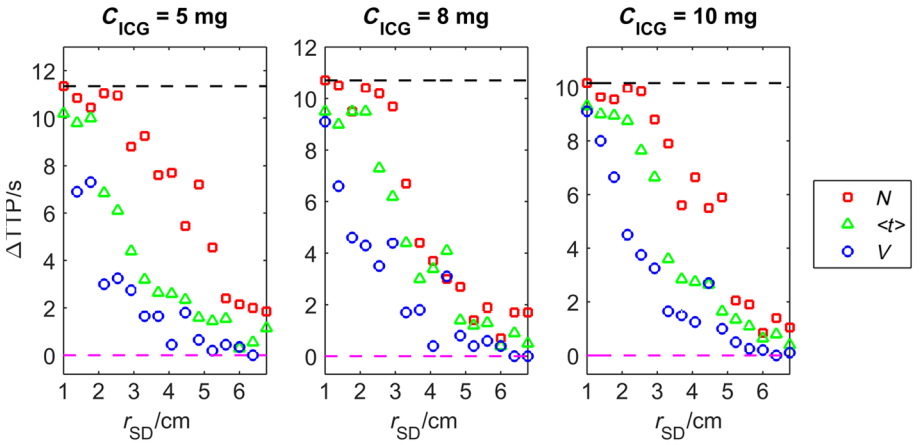

Fig. 8 Changes in ΔTTP obtained at different source-detector separations for three consecutive ICG injections in a single healthy volunteer. Different concentrations of the ICG in the bolus C_{ICG} were applied.

Additionally, in order to assess repeatability of the measurement, the analysis of moments of DTOFs obtained in consecutive injections in a single subject was performed (see Fig. 8). It can be observed that the pattern of changes in ΔTTP does not dependent significantly on the ICG concentration in the injected bolus (5, 8, and 10 mg of ICG dissolved in 5 mL of aqua pro injectione). Moreover, it can be observed that the largest delay between signals of moments obtained at different source-detector separations does not depend significantly on the dose of ICG injected.

4 Discussion

TTP is one of the mostly used parameters in perfusion CT and MRI techniques.[45–47] The TTP value is related with changes in the cerebral blood flow. It was shown that the typical value of TTP in healthy subjects is ∼17 s.[48] Number of studies showed that in patients with impaired cerebral perfusion, TTP is usually longer, and this prolongation may reach even 10 s.[49–52] Optical measurements of the delay of the contrast agent bolus passage in patients with acute ischemic stroke were carried out by Steinkellner et al.[20,21] It was shown that a small TTP prolongation (ΔTTP ≈ 4 s) in stroke hemisphere can be observed.

Analysis of dependence of TTP changes on source-detector separation was carried out by MC simulations. It shows that for the short source-detector separation, the TTP obtained from the signals representing total number of photons N reflects the inflow of the ICG to the superficial layers of the studied medium. It can be observed that TTP decreases with source-detector separations and reaches TTP_0 value related to the μ_a change modeled in the lower (intracerebral) layer of the medium. However, TTP_0 can be derived from the data obtained at shorter source-detector separations when variance V of the DTOF is analyzed. Results of the *in vivo* experiments carried out on healthy subjects show large differences (up to 12 s) between TTP calculated with the use of different statistical moments. It was noted that this variation in the TTP depends on the subject investigated. This effect can be explained by the influence of the nonhomogeneity of the extracerebral layer of the tissue on the measured DTOFs and effect of increased noise content on higher-order moments of DTOFs.[43]

Obtained results confirm once more that the higher-order statistical moments of DTOFs are more sensitive to the inflow of the dye to the deeper tissue compartments.[32] Large variation of the TTP obtained from signals representing statistical moments of DTOFs suggests that the technical aspects of data acquisition, like (1) source-detector separation, (2) order of the moment of the DTOF analyzed, and (3) number of photons acquired in a single DTOF, may significantly influence discrepancies in the TTP values derived from inflow of the ICG.

Results of this study may be useful in optimization of the measurement conditions considering the used measurement technology (available moments of the DTOFs).

5 Conclusion

The MC simulations and corresponding *in vivo* multidistance measurements show that the time-resolved monitoring during injection of the ICG may be useful in direct assessment of the intracerebral tissue hemodynamic parameters. Results of this study may be useful in optimization of the measurement conditions (source-detector distance) considering used measurement technology (available moments of the DTOFs). For continuous wave measurements (which can be modeled in time-resolved measurements by analysis of the total number of photons detected), source-detector separation at which the TTP related to the inflow of the dye to the brain can be effectively derived, and it should not be <6 cm. For source-detector separations ≥6 cm, the TTP_N derived from the signals of total number of photons is related mainly to the inflow of the dye to the brain, whereas for shorter distances, high contamination from the extracerebral tissue compartments can be observed. In case of time-resolved technique in which higher-order moments of the DTOFs (mean time of flight, variance) are available, similar results can be obtained at source-detector distance as short as 4 cm.

Acknowledgments

The studies were partly financed by the National Science Centre of Poland (NCN) in the framework of projects 2011/03/N/ST7/02598 and 2012/05/B/ST7/01162.

References

1. H. Ayaz et al., "Continuous monitoring of brain dynamics with functional near infrared spectroscopy as a tool for neuroergonomic research: empirical examples and a technological development," *Front. Hum. Neurosci.* **7**, 871 (2013).

2. F. Scholkmann et al., "A review on continuous wave functional near-infrared spectroscopy and imaging instrumentation and methodology," *NeuroImage* **85**(Pt 1), 6–27 (2014).
3. M. Wolf et al., "Functional frequency-domain near-infrared spectroscopy detects fast neuronal signal in the motor cortex," *NeuroImage* **17**(4), 1868–1875 (2002).
4. H. E. D'Arceuil et al., "Near-infrared frequency-domain optical spectroscopy and magnetic resonance imaging: a combined approach to studying cerebral maturation in neonatal rabbits," *J. Biomed. Opt.* **10**(1), 011011 (2005).
5. A. Torricelli et al., "Time domain functional NIRS imaging for human brain mapping," *NeuroImage* **85**(Pt 1), 28–50 (2014).
6. M. Ferrari and V. Quaresima, "A brief review on the history of human functional near-infrared spectroscopy (fNIRS) development and fields of application," *NeuroImage* **63**(2), 921–935 (2012).
7. B. R. White and J. P. Culver, "Quantitative evaluation of high-density diffuse optical tomography: in vivo resolution and mapping performance," *J. Biomed. Opt.* **15**(2), 026006 (2010).
8. B. W. Zeff et al., "Retinotopic mapping of adult human visual cortex with high-density diffuse optical tomography," *Proc. Natl. Acad. Sci.* **104**(29), 12169–12174 (2007).
9. A. T. Eggebrecht et al., "Mapping distributed brain function and networks with diffuse optical tomography," *Nat. Photonics* **8**(6), 448–454 (2014).
10. C. Habermehl, C. H. Schmitz, and J. Steinbrink, "Contrast enhanced high-resolution diffuse optical tomography of the human brain using ICG," *Opt. Express* **19**(19), 18636–18644 (2011).
11. N. M. Gregg et al., "Brain specificity of diffuse optical imaging: improvements from superficial signal regression and tomography," *Front. Neuroenergetics* **2**, 14 (2010).
12. T. Funane et al., "Near-infrared spectroscopy system with non-contact source and detector for in vivo multi-distance measurement of deep biological tissue," *Proc. SPIE* **8578**, 85782W (2013).
13. C. Habermehl et al., "Depth sensitivity in multi-distance NIRS measurements in humans," presented at *Biomedical Optics and 3-D Imaging*, 28 April–2 May 2012, Miami, Florida, Paper BSu3A.84, Optical Society of America, Washington, DC.
14. M. Dehaes et al., "Assessment of the frequency-domain multi-distance method to evaluate the brain optical properties: Monte Carlo simulations from neonate to adult," *Biomed. Opt. Express* **2**(3), 552–567 (2011).
15. M. A. Franceschini et al., "Assessment of infant brain development with frequency-domain near-infrared spectroscopy," *Pediatr. Res.* **61**(5 Pt 1), 546–551 (2007).
16. P. Y. Lin et al., "Non-invasive optical measurement of cerebral metabolism and hemodynamics in infants," *J. Vis. Exp.* (73), e4379 (2013).
17. S. A. Kim and S. B. Jun, "In-vivo optical measurement of neural activity in the brain," *Exp. Neurobiol.* **22**(3), 158–166 (2013).
18. V. Tsytsarev, C. Bernardelli, and K. I. Maslov, "Living brain optical imaging: technology, methods and applications," *J. Neurosci. Neuroeng.* **1**(2), 180–192 (2012).
19. A. Liebert et al., "Bed-side assessment of cerebral perfusion in stroke patients based on optical monitoring of a dye bolus by time-resolved diffuse reflectance," *NeuroImage* **24**(2), 426–435 (2005).
20. O. Steinkellner et al., "Optical bedside monitoring of cerebral perfusion: technological and methodological advances applied in a study on acute ischemic stroke," *J. Biomed. Opt.* **15**(6), 061708 (2010).
21. O. Steinkellner et al., "Cerebral perfusion in acute stroke monitored by time-domain near-infrared reflectometry," *Biocybern. Biomed. Eng.* **32**(1), 3–16 (2012).
22. W. M. Kuebler et al., "Noninvasive measurement of regional cerebral blood flow by near-infrared spectroscopy and indocyanine green," *J. Cereb. Blood Flow Metab.* **18**(4), 445–456 (1998).
23. C. Terborg et al., "Bedside assessment of cerebral perfusion reductions in patients with acute ischaemic stroke by near-infrared spectroscopy and indocyanine green," *J. Neurol. Neurosurg. Psychiatry* **75**(1), 38–42 (2004).
24. M. A. Kamp et al., "Microscope-integrated quantitative analysis of intraoperative indocyanine green fluorescence angiography for blood flow assessment: first experience in 30 patients," *Neurosurgery* **70**(1 Suppl Operative), 65–73, discussion 73–74 (2012).
25. Y. An, J. Lee, and C. Choi, "Symmetricity analysis of time to peak parameter of indocyanine green dynamics," *Proc. SPIE* **8572**, 857202 (2013).
26. A. Oldag et al., "Assessment of cortical hemodynamics by multichannel near-infrared spectroscopy in steno-occlusive disease of the middle cerebral artery," *Stroke* **43**(11), 2980–2985 (2012).
27. C. Terborg et al., "Noninvasive assessment of cerebral perfusion and oxygenation in acute ischemic stroke by near-infrared spectroscopy," *Eur. Neurol.* **62**(6), 338–343 (2009).
28. J. T. Elliott et al., "Quantifying cerebral blood flow in an adult pig ischemia model by a depth-resolved dynamic contrast-enhanced optical method," *NeuroImage* **94**(0), 303–311 (2014).
29. R. Arora et al., "Preservation of the metabolic rate of oxygen in preterm infants during indomethacin therapy for closure of the ductus arteriosus," *Pediatr. Res.* **73**(6), 713–718 (2013).
30. W. Weigl et al., "Assessment of cerebral perfusion in post-traumatic brain injury patients with the use of ICG-bolus tracking method," *NeuroImage* **85**(Pt 1), 555–565 (2014).
31. A. Liebert et al., "Time-resolved multidistance near-infrared spectroscopy of the adult head: intracerebral and extracerebral absorption changes from moments of distribution of times of flight of photons," *Appl. Opt.* **43**(15), 3037–3047 (2004).
32. J. T. Elliott et al., "Variance of time-of-flight distribution is sensitive to cerebral blood flow as demonstrated by ICG bolus-tracking measurements in adult pigs," *Biomed. Opt. Express* **4**(2), 206–218 (2013).
33. A. Liebert et al., "Assessment of inflow and washout of indocyanine green in the adult human brain by monitoring of diffuse reflectance at large source-detector separation," *J. Biomed. Opt.* **16**(4), 046011 (2011).
34. A. Liebert, H. Wabnitz, and C. Elster, "Determination of absorption changes from moments of distributions of times of flight of photons: optimization of measurement conditions for a two-layered tissue model," *J. Biomed. Opt.* **17**(5), 057005 (2012).
35. A. Liebert et al., "Monte Carlo algorithm for efficient simulation of time-resolved fluorescence in layered turbid media," *Opt. Express* **16**(17), 13188–13202 (2008).
36. D. Milej et al., "Time-resolved detection of fluorescent light during inflow of ICG to the brain—a methodological study," *Phys. Med. Biol.* **57**(20), 6725–6742 (2012).
37. D. Milej et al., "A Monte Carlo study of fluorescence generation probability in a two-layered tissue model," *Phys. Med. Biol.* **59**(6), 1407–1424 (2014).
38. T. S. Leung et al., "Theoretical investigation of measuring cerebral blood flow in the adult human head using bolus indocyanine green injection and near-infrared spectroscopy," *Appl. Opt.* **46**(10), 1604 (2007).
39. D. Milej et al., "Time-resolved multi-channel optical system for assessment of brain oxygenation and perfusion by monitoring of diffuse reflectance and fluorescence," *Opto-Electron. Rev.* **22**(1), 55–67 (2014).
40. M. Kacprzak et al., "Time-resolved optical imager for assessment of cerebral oxygenation," *J. Biomed. Opt.* **12**(3), 034019 (2007).
41. H. Wabnitz et al., "Performance assessment of time-domain optical brain imagers, part 1: basic instrumental performance protocol," *J. Biomed. Opt.* **19**(8), 086010 (2014).
42. A. Farina et al., "In-vivo multilaboratory investigation of the optical properties of the human head," *Biomed. Opt. Express* **6**(7), 2609–2623 (2015).
43. A. Liebert et al., "Evaluation of optical properties of highly scattering media by moments of distributions of times of flight of photons," *Appl. Opt.* **42**(28), 5785–5792 (2003).
44. D. Milej et al., "Advantages of fluorescence over diffuse reflectance measurements tested in phantom experiments with dynamic inflow of ICG," *Opto-Electron. Rev.* **18**(2), 208–213 (2010).
45. J. R. Reichenbach et al., "Acute stroke evaluated by time-to-peak mapping during initial and early follow-up perfusion CT studies," *Am. J. Neuroradiol.* **20**(10), 1842–1850 (1999).
46. A. Kheradmand, M. Fisher, and D. Paydarfar, "Ischemic stroke in evolution: predictive value of perfusion computed tomography," *J. Stroke Cerebrovasc. Dis.* **23**(5), 836–843 (2014).
47. B. C. Campbell et al., "Comparison of computed tomography perfusion and magnetic resonance imaging perfusion-diffusion mismatch in ischemic stroke," *Stroke* **43**(10), 2648–2653 (2012).
48. B. F. Tomandl et al., "Comprehensive imaging of ischemic stroke with multisection CT," *RadioGraphics* **23**(3), 565–592 (2003).

49. K. Kajimoto et al., "Cerebral hemodynamic evaluation using perfusion-weighted magnetic resonance imaging: comparison with positron emission tomography values in chronic occlusive carotid disease," *Stroke* **34**(7), 1662–1666 (2003).
50. J. M. Olivot et al., "Perfusion MRI (Tmax and MTT) correlation with xenon CT cerebral blood flow in stroke patients," *Neurology* **72**(13), 1140–1145 (2009).
51. J. Zhang et al., "Whole-brain CT perfusion and CT angiography assessment of moyamoya disease before and after surgical revascularization: preliminary study with 256-slice CT," *PLoS One* **8**(2), e57595 (2013).
52. J. W. Dankbaar et al., "Diagnostic threshold values of cerebral perfusion measured with computed tomography for delayed cerebral ischemia after aneurysmal subarachnoid hemorrhage," *Stroke* **41**(9), 1927–1932 (2010).

Daniel Milej is a postdoctoral fellow at Western University in London, Canada, and a researcher at Lawson Health Research Institute in London, Canada. He received his MSc degree in optoelectronics from Military University of Technology, Warsaw, in 2008 and his PhD in biomedical engineering optics from the Nalecz Institute of Biocybernetics and Biomedical Engineering, Polish Academy of Sciences in 2014. He is the author and coauthor of 16 journal papers and two book chapters. His current research areas include time-domain optical brain imaging, functional near-infrared spectroscopy, fluorescence measurements, development of instrumentation, and clinical applications.

Biographies for the other authors are not available.